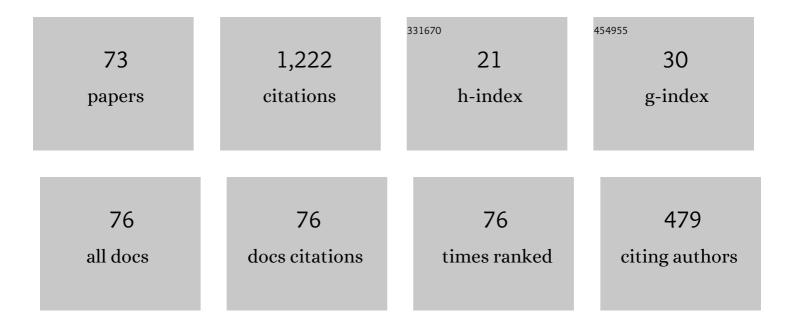
Sheng-ping He

List of Publications by Year in descending order

Source: https://exaly.com/author-pdf/8695333/publications.pdf Version: 2024-02-01



SHENC-DINC HE

#	Article	IF	CITATIONS
1	Molecular dynamics simulation of the structure and properties for the CaO–SiO2 and CaO–Al2O3 systems. Journal of Non-Crystalline Solids, 2015, 411, 145-151.	3.1	74
2	Structural and viscosity properties of CaO-SiO 2 -Al 2 O 3 -FeO slags based on molecular dynamic simulation. Journal of Non-Crystalline Solids, 2016, 450, 23-31.	3.1	67
3	Study on Properties of Aluminaâ€Based Mould Fluxes for Highâ€Al Steel Slab Casting. Steel Research International, 2012, 83, 1194-1202.	1.8	63
4	Mineral Change of Philippine and Indonesia Nickel Lateritic Ore during Sintering and Mineralogy of Their Sinter. ISIJ International, 2010, 50, 380-385.	1.4	44
5	Investigation of the Air-Argon-Steel-Slag Flow in an Industrial RH Reactor with VOF–DPM Coupled Model. Metallurgical and Materials Transactions B: Process Metallurgy and Materials Processing Science, 2017, 48, 2176-2186.	2.1	42
6	Properties of High Basicity Mold Fluxes for Peritectic Steel Slab Casting. Journal of Iron and Steel Research International, 2012, 19, 39-45.	2.8	40
7	Molecular dynamics simulations of the structural properties of Al2O3-based binary systems. Journal of Non-Crystalline Solids, 2016, 435, 17-26.	3.1	35
8	Effect of Fluorine on the Structure of High Al2O3-Bearing System by Molecular Dynamics Simulation. Metallurgical and Materials Transactions B: Process Metallurgy and Materials Processing Science, 2015, 46, 2005-2013.	2.1	34
9	Thermodynamics of Complex Sulfide Inclusion Formation in Ca-Treated Al-Killed Structural Steel. Metallurgical and Materials Transactions B: Process Metallurgy and Materials Processing Science, 2016, 47, 2549-2557.	2.1	33
10	Mixing behavior in the RH degasser with bottom gas injection. Vacuum, 2016, 130, 48-55.	3.5	33
11	Morphology Control for Al2O3 Inclusion Without Ca Treatment in High-Aluminum Steel. Metallurgical and Materials Transactions B: Process Metallurgy and Materials Processing Science, 2015, 46, 585-594.	2.1	32
12	Investigation of Gas and Liquid Multiphase Flow in the Rheinsahl–Heraeus (RH) Reactor by Using the Euler–Euler Approach. Jom, 2016, 68, 2138-2148.	1.9	30
13	Structure investigation of CaO-SiO2-Al2O3-Li2O by molecular dynamics simulation and Raman spectroscopy. Journal of Non-Crystalline Solids, 2019, 526, 119695.	3.1	29
14	Effect of Substituting CaO with BaO and CaO/Al2O3 Ratio on the Viscosity of CaO–BaO–Al2O3–CaF2–Li2O Mold Flux System. Metals, 2019, 9, 142.	2.3	29
15	Study on Reaction Performances and Applications of Mold Flux for High-Aluminum Steel. Materials Transactions, 2016, 57, 58-63.	1.2	27
16	Molecular Dynamics Simulation of the Structure and Properties of CaO-SiO2-CaF2 Slag Systems. Metallurgical and Materials Transactions B: Process Metallurgy and Materials Processing Science, 2019, 50, 1503-1513.	2.1	25
17	Review of Mold Fluxes for Continuous Casting of Highâ€Alloy (Al, Mn, Ti) Steels. Steel Research International, 2019, 90, 1800424.	1.8	25
18	Desulphurisation Process in RH Degasser for Soft-killed Ultra- low-carbon Electrical Steels. ISIJ International, 2012, 52, 977-983.	1.4	24

SHENG-PING HE

#	Article	IF	CITATIONS
19	Solidification and crystallization properties of CaO-SiO2-Na2O based mold fluxes. International Journal of Minerals, Metallurgy and Materials, 2009, 16, 261-264.	4.9	23
20	Electrical Conductivity, Viscosity and Structure of CaO–Al2O3-Based Mold Slags for Continuous Casting of High-Al Steels. Metallurgical and Materials Transactions B: Process Metallurgy and Materials Processing Science, 2021, 52, 2526-2535.	2.1	23
21	Dissolution behaviour of Al2O3 in mould fluxes with low SiO2 content. Ceramics International, 2019, 45, 4035-4042.	4.8	22
22	Effect of Elements on Peritectic Reaction in Molten Steel Based on Thermodynamic Analysis. ISIJ International, 2012, 52, 1856-1861.	1.4	21
23	Effect of Exit Shape of Submerged Entry Nozzle on Flow Field and Slag Entrainment in Continuous Casting Mold. Metallurgical and Materials Transactions B: Process Metallurgy and Materials Processing Science, 2020, 51, 2862-2870.	2.1	21
24	Effects of the amphoteric behavior of Al2O3 on the structure and properties of CaO–SiO2–Al2O3 melts by molecular dynamics. Journal of Non-Crystalline Solids, 2021, 552, 120435.	3.1	21
25	Study of the Mechanism of Liquid Slag Infiltration for Lubrication in Slab Continuous Casting. Metallurgical and Materials Transactions B: Process Metallurgy and Materials Processing Science, 2018, 49, 2038-2049.	2.1	20
26	Modeling Dynamics of Agglomeration, Transport, and Removal of Al ₂ O ₃ Clusters in the Rheinsahl–Heraeus Reactor Based on the Coupled Computational Fluid Dynamics-Population Balance Method Model. Industrial & Engineering Chemistry Research, 2016, 55, 7030-7042.	3.7	18
27	Effect of Transition Metal Oxides on Radiative Heat Transfer through Mold Flux Film in Continuous Casting of Steel. ISIJ International, 2007, 47, 1294-1299.	1.4	17
28	Dissolution behavior of Al2O3 into tundish slag for high-al steel. Journal of Materials Research and Technology, 2020, 9, 11311-11318.	5.8	16
29	Solidification Properties of CaO-SO2-TiO2 Based Mold Fluxes. Journal of Iron and Steel Research International, 2011, 18, 15-19.	2.8	15
30	Assessment of an Eulerian multi-fluid VOF model for simulation of multiphase flow in an industrial Ruhrstahl–Heraeus degasser. Metallurgical Research and Technology, 2019, 116, 617.	0.7	14
31	The relationship between crystallization and break temperature of mould flux. Ironmaking and Steelmaking, 2019, 46, 865-871.	2.1	14
32	Structure of Solidified Films of Mold Flux for Peritectic Steel. Metallurgical and Materials Transactions B: Process Metallurgy and Materials Processing Science, 2017, 48, 1652-1658.	2.1	13
33	Investigation of mixing and slag layer behaviours in the RH degasser with bottom gas injection by using the VOF–DPM coupled model. Ironmaking and Steelmaking, 2019, 46, 771-776.	2.1	13
34	Analysis of Crack Susceptibility of Regular Carbon Steel Slabs Using Volume-Based Shrinkage Index. ISIJ International, 2013, 53, 1812-1817.	1.4	12
35	Study of Non-Newtonian Behavior of CaO-SiO2-Based Mold Slag and Its Effect on Lubrication in Continuous Casting of Steel. Metallurgical and Materials Transactions B: Process Metallurgy and Materials Processing Science, 2019, 50, 1052-1059.	2.1	12
36	Volatilisation problems in the measurement of mould fluxes crystallisation by hot thermocouple technique. Ironmaking and Steelmaking, 2019, 46, 141-147.	2.1	12

SHENG-PING HE

#	Article	IF	CITATIONS
37	Mechanism of Floater Formation in the Mold during Continuous Casting of Ti-Stabilized Austenitic Stainless Steels. Metals, 2019, 9, 635.	2.3	11
38	Application of Inhomogeneous Discrete Method to the Simulation of Transport, Agglomeration, and Removal of Oxide Inclusions in a Gas-Stirred Ladle. Jom, 2019, 71, 4206-4214.	1.9	11
39	Structure Evolution of Slag Films of Ultrahigh-Basicity Mold Flux During Solidification. Metallurgical and Materials Transactions B: Process Metallurgy and Materials Processing Science, 2017, 48, 1938-1942.	2.1	10
40	Wetting and Erosion of ZrO2-Graphite Refractory by CaO-SiO2 and CaO-Al2O3-Based Mold Slags for Submerged Entry Nozzle. Metallurgical and Materials Transactions B: Process Metallurgy and Materials Processing Science, 2019, 50, 1407-1416.	2.1	10
41	Contact angle and adhesion of CaO-SiO2- and CaO-Al2O3-based mold slags on solid steel of various compositions. Journal of Materials Research and Technology, 2020, 9, 7828-7837.	5.8	10
42	Castability of aluminum- and sulfur-bearing free-cutting steel. Journal of Iron and Steel Research International, 2015, 22, 87-92.	2.8	9
43	Optimization of calcium addition to high-strength low-alloy steels. Journal of Iron and Steel Research International, 2015, 22, 590-597.	2.8	9
44	Circulation flow rate and decarburization in the RH degasser under low atmospheric pressure. Vacuum, 2018, 153, 132-138.	3.5	9
45	In situ observation of crystallization of mold slag using a digital optical microscope in an infrared furnace. Journal of the American Ceramic Society, 2019, 102, 104-108.	3.8	9
46	Mold Nonsinusoidal Oscillation Mode and Its Effect on Slag Infiltration for Lubrication and Initial Shell Growth during Steel Continuous Casting. Metals, 2019, 9, 418.	2.3	9
47	Numerical simulation of Argon–Molten steel two-phase flow in an industrial single snorkel refining furnace with bubble expansion, coalescence, and breakup. Journal of Materials Research and Technology, 2020, 9, 3318-3329.	5.8	9
48	Thermodynamic and experimental study on CO2 injection in RH decarburization process of ultra-low carbon steel. Journal of CO2 Utilization, 2021, 50, 101586.	6.8	9
49	Effect of TiO2 substituting SiO2 on the rheological and crystallization behavior of mold slags for casting Ti-containing steel. Ceramics International, 2022, 48, 256-265.	4.8	9
50	Influence of Submerged Entry Nozzle Clogging on the Flow Field and Slag Entrainment in the Continuous Casting Mold by the Physical Model. Metallurgical and Materials Transactions B: Process Metallurgy and Materials Processing Science, 2022, 53, 1436-1445.	2.1	9
51	Effect of FeO content in Slag on formation of MgOfflAl ₂ O ₃ inclusion for Al-killed steel. Metallurgical Research and Technology, 2016, 113, 204.	0.7	8
52	Effect of Interfacial Reaction between CaO–BaO–Al ₂ O ₃ â€Based Mold Fluxes and Highâ€Mn–Highâ€Al Steels on Fundamental Properties and Lubrication of Mold Flux. Steel Research International, 2020, 91, 1900581.	1.8	7
53	Influence of Interfacial Thermal Resistance on Initial Solidification and Heat Transfer in Continuous Casting Mold of Steel. Steel Research International, 2021, 92, 2000636.	1.8	7
54	Properties and structure of a new non-reactive mold flux for high-Al steel. Journal of Iron and Steel Research International, 2022, 29, 61-70.	2.8	7

Sheng-ping He

#	Article	IF	CITATIONS
55	Modeling Fluid Flow and Carbon Removal in the Ruhrstahl–Heraeus Reactor: Considering the Pumping Process. Industrial & Engineering Chemistry Research, 2019, 58, 18855-18865.	3.7	6
56	Thermodynamic Discussion of CO 2 Injection in Molten Steel. Steel Research International, 2020, 91, 1900450.	1.8	6
57	Hydrodynamic Modeling of Two-Phase Flow in the Industrial Ruhrstahl–Heraeus Degasser: Effect of Bubble Expansion Models. Metallurgical and Materials Transactions B: Process Metallurgy and Materials Processing Science, 2022, 53, 208-219.	2.1	6
58	Effects of Substituting SiO ₂ with Oxidisers on the Reaction Performance and Physical Properties of Mould Flux for High Ti-bearing Steel. ISIJ International, 2021, 61, 814-823.	1.4	5
59	3D Coupled Model on Dynamic Initial Solidification and Slag Infiltration at the Corner of Slab Continuous Casting Mold. Steel Research International, 2021, 92, 2100101.	1.8	5
60	Amphoteric behavior of component and microstructure feature on CaO-Al2O3-TiO2 ternary melt by molecular dynamics simulation. Computational Materials Science, 2022, 205, 111223.	3.0	5
61	Effect of the Charging Temperature on the Hot Ductility of Nbâ€Containing Steel in the Simulated Hot Charge Process. Steel Research International, 2012, 83, 671-677.	1.8	4
62	Reaction performances of mould slags with different SiO2 contents for 321 stainless steel. Canadian Metallurgical Quarterly, 2019, 58, 464-470.	1.2	4
63	Investigation of rheological behavior for commercial mold slags. Journal of Materials Research and Technology, 2020, 9, 9568-9575.	5.8	4
64	Effects of Transition Metal Oxides ZrO2, Y2O3, and Sc2O3 on Radiative Heat Transfer of Low-Reactive CaO-Al2O3-Based Mold Slag. Metallurgical and Materials Transactions B: Process Metallurgy and Materials Processing Science, 2020, 51, 677-689.	2.1	4
65	Development of Test Method for Measuring Sintering Temperature of Mould Fluxes. Journal of Iron and Steel Research International, 2011, 18, 1-6.	2.8	3
66	Structure of Solidified Films of CaO-SiO2-Na2O Based Low-Fluorine Mold Flux. Metals, 2019, 9, 93.	2.3	3
67	Study of Thermodynamic for Low-Reactive CaO-BaO-Al2O3-SiO2-CaF2-Li2O Mold Flux Based on the Model of Ion and Molecular Coexistence Theory. Metals, 2022, 12, 1099.	2.3	3
68	Mathematical Modeling of Heat Transfer and Deformation of Bloom Tube Mold in Continuous Casting Process. Metallurgical and Materials Transactions B: Process Metallurgy and Materials Processing Science, 2020, 51, 213-221.	2.1	2
69	Thermodynamic Properties of the FeS–MnS–CuS0.5 Ternary System at 1473 K. ISIJ International, 2013, 53, 966-972.	1.4	2
70	Effect of Dispersant on the Dispersibility of CaO–Al2O3-Based Mold Powder Slurry. Transactions of the Indian Institute of Metals, 2022, 75, 473-479.	1.5	2
71	Effect of (BaO+CaO)/Al2O3 ratio (1.7â^¼2.0) on the structure and Al-Li association of BaO-CaO-Al2O3-CaF2-Li2O mold flux. Journal of Non-Crystalline Solids, 2022, 584, 121522.	3.1	2
72	Investigation and Minimization of Slag Spot Surface Defects in Continuous Casting of High Carbon Steel Billets through Statistical Evaluation. Metals, 2020, 10, 878.	2.3	1

#	Article	IF	CITATIONS
73	Effect of MgO on solidification and crystallization properties of ultrahigh-basicity mold flux. Materials Chemistry and Physics, 2021, , 125403.	4.0	Ο